2013

Experimental study and modeling of a novel magnetorheological elastomer isolator

Jian Yang
University of Wollongong, jy937@uowmail.edu.au

Haiping Du
University of Wollongong, hdu@uow.edu.au

Weihua Li
University of Wollongong, weihuali@uow.edu.au

Yancheng Li
University Of Technology Sydney

Jianchun Li
University Of Technology Sydney

See next page for additional authors

Publication Details

Yang, J., Du, H., Li, W., Li, Y., Li, J., Sun, S. & deng, H. X. (2013). Experimental study and modeling of a novel magnetorheological elastomer isolator. Smart Materials and Structures, 22 (11), 1-14.

Experimental study and modeling of a novel magnetorheological elastomer isolator

Abstract
This paper reports an experimental setup aiming at evaluating the performance of a newly designed magnetorheological elastomer (MRE) seismic isolator. As a further effort to explore the field-dependent stiffness/damping properties of the MRE isolator, a series of experimental testing were conducted. Based upon the analysis of the experimental responses and the characteristics of the MRE isolator, a new model that is capable of reproducing the unique MRE isolator dynamics behaviors is proposed. The validation results verify the model's effectiveness to portray the MRE isolator. A study on the field-dependent parameters is then provided to make the model valid with fluctuating magnetic fields. To fully explore the mechanism of the proposed model, an investigation relating the dependence of the proposed model on every parameter is carried out.

Keywords
isolator, experimental, modeling, study, novel, magnetorheological, elastomer

Disciplines
Engineering | Science and Technology Studies

Publication Details
Yang, J., Du, H., Li, W., Li, Y., Li, J., Sun, S. & deng, H. X. (2013). Experimental study and modeling of a novel magnetorheological elastomer isolator. Smart Materials and Structures, 22 (11), 1-14.

Authors
Jian Yang, Haiping Du, Weihua Li, Yancheng Li, Jianchun Li, Shuaishuai Sun, and H X. deng

Experimental Study and Modeling of a Novel Magnetorheological Elastomer Isolator

Jian Yang[1], Haiping Du[2], Weihua Li*[1], Yancheng Li[3], Jianchun Li[3], Shuaishuai Sun[1], and H.X. Deng[4]*

1. School of Mechanical, Material and Mechatronic Engineering, University of Wollongong, NSW 2522, Australia

2. School of Electrical, Computer and Telecommunications Engineering, University of Wollongong, NSW 2522, Australia

3. Centre for Built Infrastructure Research, School of Civil and Environmental Engineering, Faculty of Engineering and Information Technology, University of Technology, Sydney, NSW 2007, Australia

4. School of Instrument Science and Opto-electronics Engineering, Hefei University of Technology, Hefei, Anhui, 230009, P.R.China

E-mails: hdu@uow.edu.au; weihuali@uow.edu.au

Abstract

This paper reports an experimental setup aiming at evaluating the performance of a newly designed magnetorheological elastomer (MRE) seismic isolator. As a further effort to explore the field-dependent stiffness/damping properties of the MRE isolator, a series of experimental testing were conducted. Upon on the analysis of the experimental responses and the characteristics of the MRE isolator, a new model that is capable of reproducing the unique MRE isolator dynamics behaviors is proposed. The validation results verify the model's effectiveness to portray the MRE isolator. A study on the field-dependent parameters is then provided to make the model valid with fluctuating magnetic fields. To fully explore the mechanism of the proposed model, an investigation relating the dependence of the proposed model on every parameter is carried out.

Keywords: Magnetorheological elastomer, isolator, modeling, parameter identification

1. Introduction

Semi-active control devices have been extensively used for vibration reduction in civil engineering structures and vehicle suspensions because of their superiority of offering the versatility of fully active control and reliability of passive control. Active control devices appear to be an ideal strategy for the great isolation performances, however, disadvantages arise when it refers to cost, power requirement and complexity [1]. Passive control devices gain compliments for their simplicity and ease of implementation, nevertheless, the limitation of inadaptability make them fail to satisfy the advanced requirements. Semi-active control devices fill the gap in that they possess the advantages of both fully active control and passive control devices [2]. Furthermore, semi-active control devices can achieve parameter adjustment in real time without requiring a large power. Over the past decades, semi-active

control devices have attracted considerable attention due to their high adaptability. Applications of such devices have been considered for vibration control in automobile industry and civil engineering including variable orifice dampers [3], controllable friction braces [4], controllable friction isolators [5], variable stiffness devices [6] and electrorheological (ER) dampers [7].

In order to give a full play to the potentials of semi-active devices, significant efforts have been conducted to the possibility of incorporating smart materials into the semi-active devices for vibration reduction. Among the well-established family of smart materials resides a sub-class of materials known as 'field responsive fluids' including electrorheological (ER) fluids and magnetorheological (MR) fluids. They are outstanding from traditional smart materials mainly because of their soft morphology and their controllable rheology by an external electric or magnetic field. ER fluids and MR fluids both date back to 1940's, however, primary research has focused on the development of ER fluids and devices. The new and emerging MR fluids appear to be a superior alternative to ER fluids because MR fluids handle with many drawbacks associated with ER fluids, including lower yield stress, temperature dependence, sensitivity to impurities and relatively high voltage supplies. Furthermore, MR fluids can achieve rheological transition within a few milliseconds and can exhibit viscoelastic properties when exposed to a magnetic field. To date, various semi-active devices using MR fluids have been developed, among which, MR dampers that offer reliable and stable operations at a modest cost have been extensively used in a wide range from civil structures such as buildings and bridges [8] to automobiles [9] and railway vehicles [10]. For several decades, considerable researches have been going into modeling MR dampers. The Bingham model was first proposed for an ER damper [11] and then an attempt was made to use it to describe MR damper [12]. However, it turned out Bingham model failed to capture the nonlinear force-velocity relationships of MR damper. Compared with the Bingham model, the Bouc-Wen model was able to predict the force-displacement response very well but was unable to capture the force-velocity behavior in some specific regions. To optimize the performance of the Bouc-Wen model, a modified version was proposed for MR damper that addressed the disadvantages associated with the previously considered models. For decades the modified Bouc-Wen model has been generally accepted to describe a MR damper because it predicts MR damper behaviors very well in all regions.

In addition to MR fluids, MR elastomers (MREs) are another class of MR materials. The solid state of MRE overcomes the disadvantages of liquid leakage and particle residue due to the liquid state of MR fluids. To this end, they are now classified as such kind of smart materials particularly well suited to provide effective performance in structural control. Typical MREs consist of three components named polarized particles, matrix and additives. These polarized particles are suspended in a non-magnetic solid or gel-like matrix. When a magnetic field is applied MRE performs field dependent stiffness and damping properties [13]. The unique merits of MRE relate directly to its practical applications for vibration control. For example, MREs have been used to provide variable stiffness in automobile engine suspension system [14] or vehicle seat suspension system [15]. Also, MREs are used to construct adaptive tuned vibration absorbs [16-18].

To date, a more general use of MR elastomers is to be incorporated into an isolator device. Different from MR dampers, in addition to controllable damping, MRE isolators also achieve controllable modulus, for this reason, many researchers have devoted to explore the potential of MRE isolator in mitigating undesired structural or machinery vibrations [14, 16, 19]. Li, *et al.* designed and fabricated an adaptive MRE seismic isolator which achieves a significant adjustable range of lateral stiffness under a medium level of magnetic field [20]. The designed MRE seismic isolator outperforms the traditional seismic isolator in terms of the effectiveness and functionality for the seismic protection of civil structures. Compared to MR damper, relatively less research work has been done when it refers to model development of MRE devices. A four-parameter viscoelastic model for MRE was proposed in [21], however, it is limited to present the linear relationship of force and displacement. Therefore, ongoing research should spare no effort to develop a model for MRE isolator, and evaluate its performance in vibration control.

To further explore the unique potentials of MRE isolator and make them fully utilized in vibration mitigation of structural or machinery, a highly adaptive MRE seismic isolator was designed and fabricated [22] for evaluating MRE isolator nonlinear behaviors. The main contributions of this work include: (a) a novel design of the multiplayer MRE isolator; and (b) a new phenomenological model to precisely predict MRE isolator nonlinear responses. Specifically, the experiment part given in Section 2 includes the design of multiplayer MRE-based seismic isolator and magnetic circuit, the experimental setup, and the analyses for the unique MRE isolator responses. Based on the understanding of MRE isolator behaviors, a model that is adequate to portray this device is proposed and validated in Section 3. Additionally, in Section 4, the effect of every single parameter on the model output is discussed.

2. Experimental Setup and Testing

2.1 Configuration of the MRE seismic isolator

A prototype of a novel MRE base isolator was designed and fabricated [20]. The configuration of the MRE isolator, as shown in Figure 1, incorporates the laminated structural design of traditional laminated rubber bearing [22]. It consists of multilayer thin MRE sheets bonded onto multilayer thin steel plates. In this design, there are 26 layers of the steel sheet with a thickness of 1 mm and 25 layers of MRE sheets with a thickness of 1 mm being used. The diameter of the MRE and steel sheets is 120 mm.

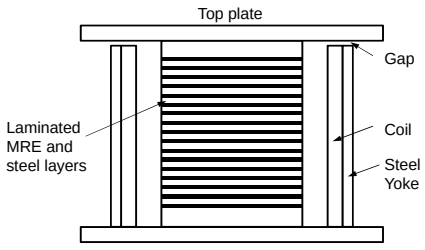

Figure 1. Cross section of the MRE seismic isolator.

In the design, the laminated bearing element is placed inside of a solenoid, which generates magnetic field after it is energized with electric currents. The solenoid is made of electromagnetic coil and thin non-magnetic support as illustrated in Figure 1. The cylindrical shape non-magnetic support is made of epoxy material and has an inner diameter of 146 mm and a thickness of 2 mm. The cylindrical electromagnetic coil has an inner diameter of 150 mm and an outer diameter of 200 mm. The coil is firmly attached to the epoxy support. The diameter of the coil wire is 1.0 mm with a total winding number of 2900 turns. The wire made of copper has an electric resistance of 42.3 Ω. The space between the laminated MRE structure and the coil enables the MRE isolator to have a maximum deformation of 15 mm, equivalent to the maximum allowable shear strain of 60%.

2.2 Magnetic circuit design

In the design of the highly adaptive MRE isolator, one innovation is the laminated structure consisting of 25 layers of MRE sheets sandwiched between 26 layers of steel plates. As can been seen from Figure 2, the MRE material is placed inside of the magnetic coil, serving as the magnetic core of the magnetic circuit. Comparing with the weak and divergent magnetic field outside of the coil, the magnetic field inside the solenoid is strong and uniform. The major advantage of this design is that it creates a large effective area that is essential for MRE base isolator design. The MRE material inside the solenoid can be fully energized by a uniform magnetic field. However, due to the low permeability of the MRE material, the configuration needs to be modified in actual design to increase the permeability of the magnetic coil for which MRE forms a part of it.

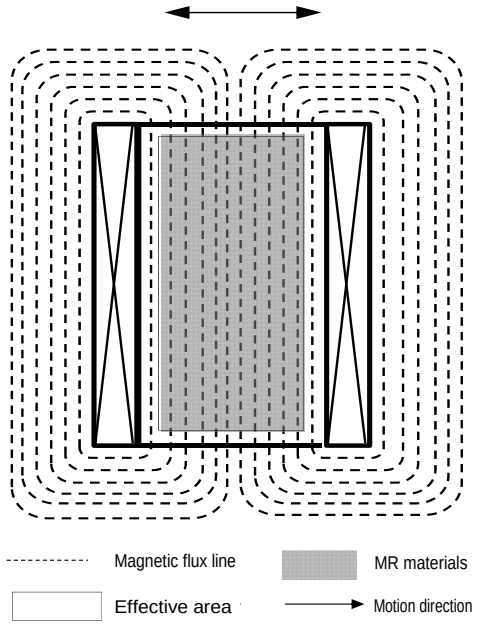

Figure 2. Invention design of magnetic circuit

2.3 Experimental setup

To evaluate and characterize the performance of the MRE base isolator prototype, a series of experimental tests were conducted. Figure 3 shows the schematic of the experimental set-up, where a shake table, which is available in the University of Technology, Sydney, was used to provide horizontal loadings to the isolator either in the quasi-static mode or in dynamic mode. The MRE base isolator was mounted on the shake table and moves along with the shake table motion. A load cell (Model No. STS-300-B10, Sun Scale INC) was installed to a fixed reaction rig to measure the lateral load applied to the isolator. During the test, the top plate of the MRE isolator and the load cell remain motionless thus eliminate the undesired inertia force in the measurements. A displacement sensor (MTS, USA) was used to measure provides the displacement. A DC power supply (DC Power Conditioner, SOLA Electric, Division of SOLA Basic Australia) with a capacity of 240V and 5.3A, as shown in Figure 4, provides DC current to energize the magnetic coil. A slider (Type: S-260-10, Yamabishi Electric Co. Ltd, Tokyo, Japan) was used to adjust the applied current to the magnetic coil, also shown in Figure 4. A multi-meter (Model No. 115, Fluke) was also used to monitor the current output from the slider during the testing.

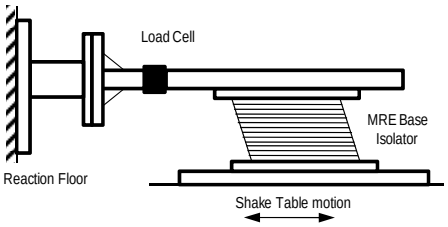

Figure 3. Sketch diagram of the experimental set-up.

Figure 4. MRE seismic isolator during testing and equipments (power conditioner and the slider).

In this study, a series of preliminary tests were conducted to measure the response of the damper under various loading conditions. In each test, the MRE isolator was driven with a sinusoidal signal with a fixed frequency, and the current applied to the MRE isolator was held at a constant level. A wide range of frequencies (0.1Hz, 1.0Hz, 2.0Hz, and 4.0Hz), amplitudes (2mm, 4mm, and 8mm, corresponding to shear strain of 8%, 16%, and 32%), and currents (0A, 1A, 2A, and 3A) are considered. The sampling rate for the data acquisition was set at 256 Hz for capturing all test results including the dynamic tests. The velocity response was calculated from the measured displacements using a central difference method.

2.4 Testing results

Figure 5 shows the responses of force-displacement (Figure 5(a)) and force-velocity (Figure 5(b)) when the MRE isolator was loaded with the sinusoidal signal of three amplitudes (2 mm, 4mm and 8mm) at constant frequency (4 Hz) and current (2 A). The effects of changing the amplitudes are clearly observed. On one hand, it is observed from Figure 5(a) that the maximum force and the equivalent damping, indicated by the area enclosed by the force-displacement loop, gain a large increase with the increasing amplitude. Also it is noted that the nonlinear relationship between force and velocity appears much more obvious when the amplitude is large, as shown in Figure 5(b). On the other hand, a closer observation on the hysteresis loops reveals that the effective stiffness of the MRE isolator, represented by the slope of force-displacement loop, decreases slightly with ascending loading amplitudes. This physical phenomenon is called Mullins Effect, which was first studied by Holt [23] and further examined by Mullins [24, 25].

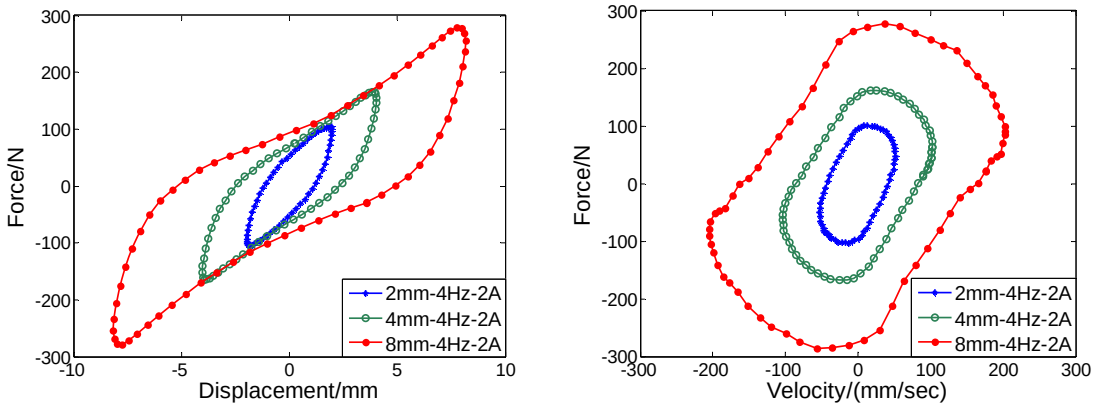

(a) Force vs. displacement (b) Force vs. velocity

Figure 5. Experimental responses of the MRE isolator under sinusoidal inputs with different amplitudes.

Mullins Effect is explained that if a rubber is stretched to a relative elongation and released, it will not follow the same stress-strain curve when it is stretched once again. Instead, the rubber appears to be much softer on the second stretch. The physical meaning of Mullins effect is the strain softening behavior of the elastomer when increase the loading amplitude, indicated by the descending stiffness for ascending amplitude cases [26].

The effects of changing frequencies on performance of the MRE isolator are presented in Figure 6. It is noticed from Figure 6 (a) that frequencies have a slight influence on the maximum force and effective stiffness. In particular, in the cases when the frequencies are above 0.1Hz the measured force and effective stiffness almost remain independent of frequency. Similar to amplitudes, the ascending frequencies induce an increasing nonlinearity of force-velocity relationship.

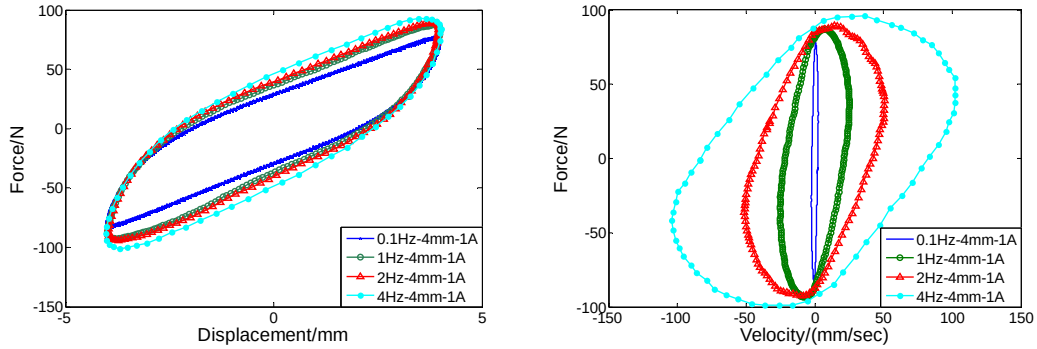

(a) Force vs. displacement (b) Force vs. velocity

Figure 6. Experimental responses of the MRE isolator under sinusoidal inputs with different frequencies.

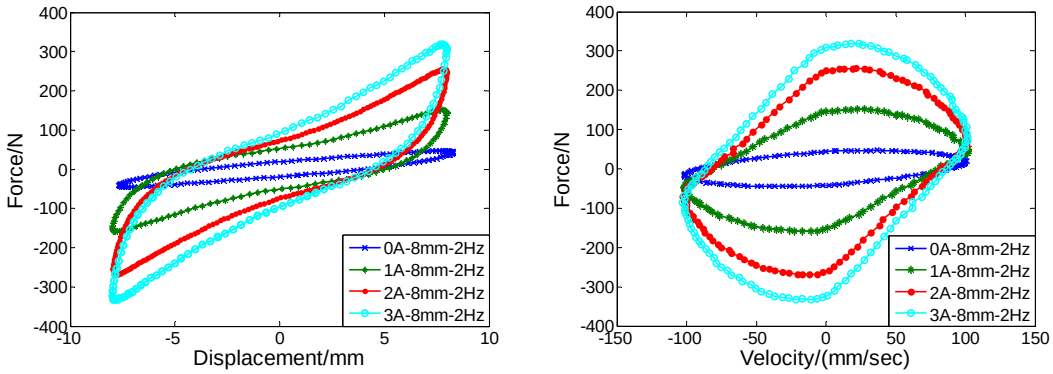

(a) Force vs. displacement (b) Force vs. velocity

Figure 7. Experimental responses of the MRE isolator under sinusoidal inputs with different currents.

The response of the MRE isolator based on a 2 Hz sinusoid with an amplitude of 8mm is shown in Figure 7 for four constant current levels, 0 A, 1A, 2 A, and 3 A. At the 0 A level, the force-displacement relationship is approximately elliptical, and the force-velocity relationship is nearly linear. However, as the current level increases, the strain stiffening phenomenon shown in Figure 7(a) and the nonlinear response of force-velocity illustrated in Figure 7(b) appear to be evident. Also, the increase in the force-displacement loop area and the effective stiffness demonstrates that the damping capacity and shear modulus of MRE are functions of the applied current.

Another property to be noted in the experimental data is strain stiffening which is obvious when the amplitude is large. The explanation for strain stiffening is attributed to the limited extensibility of the polymer chains [27] for normal rubber. However, for the field-dependent MRE cases, it is much more complicated. When a certain current level is applied to the MRE, in addition to the resistance of rubber matrix, the iron particles are also held by the magnetic force from the surrounding iron particle, which makes the extensibility of the chain structure even less. This explains some cases where the strain stiffening is minimal for zero field situations but is obvious for nonzero magnetic field, as illustrated in Figure 7(a).

In the next section, a new phenomenological model for the MRE isolator will be proposed and evaluated.

3. Modelling and Validation

In modeling the MRE isolator responses, a major challenge is being able to capture the strain stiffening in force-displacement loops and the nonlinear relationship between force and velocity. To accurately portray these unique behaviors of the MRE isolator, a new phenomenological model is proposed in this section as shown in Figure 8. This model incorporates a Bouc-Wen component, which reproduces hysteresis loops, in parallel with a Viogt element, which describes solid-material behaviors. The Bouc-Wen component is described by the evolutionary variable z that represents a function of the time history of the displacement. It is widely accepted in structure engineering and MR behavior for its mathematical simplicity and ability to represent a large class of hysteretic behavior. In this work, the Bouc-Wen component combined with a spring and a damper is used to portray the unique field dependent stiffness/damping properties of MRE isolator. The force of this system is given by:

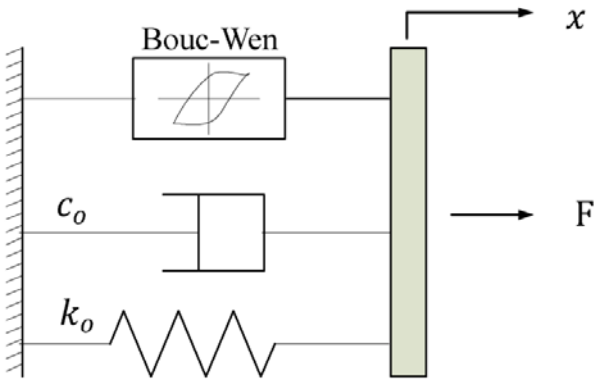

Figure 8. Schematic diagram of the proposed MRE isolator model.

$$F = \alpha k_0 x + (1-\alpha) k_0 z + c_0 \dot{x} \ , \tag{1}$$

where the evolutionary variable z is described as:

$$\dot{z} = A\dot{x} - \beta|\dot{x}||z|^{n-1}z - \gamma\dot{x}|z|^{n}, \tag{2}$$

k_0 is the stiffness of the spring, and c_0 represents the viscous coefficient indicating the damping capacity of the system. The item of $c_0\dot{x}$ is a component of the total force. The rest part represents the restoring force as the summation of a linear component $\alpha k_0 x$ and a purely hysteretic component $(1-\alpha)k_0 z$, in which $\alpha \in (0,1)$ represents the linearity level of the hysteresis loops. In Eq. (2), A, n, β and γ, which are non-dimensional parameters, are responsible for the shape and the size of the hysteresis loops. The parameter A has a big influence on the maximum force, and n is recognized to control the transition from linear to nonlinear range. In this work, the value of $n = 1$ is considered for the purpose of reducing the overall number of system unknowns in the identification process on the ground that the

chosen value satisfies the fitting requirements. β and γ mainly shape the hysteresis loops. Different combinations of the signs of $\beta+\gamma$ and $\beta-\gamma$ reproduce different shapes of hysteresis loops. A detailed investigation has been done in [28], where five kinds of hysteresis loops corresponding to five combinations of the signs of $\beta+\gamma$ and $\beta-\gamma$ have been presented.

To evaluate the model's effectiveness to predict the MRE isolator performances, a set of parameters are identified for the model to fit the experimental data shown in Figure 5 (8mm-amplitude, 4Hz-frequency, and 2A current). The optimal values are listed in Table 1. In the identification process, there are in total 6 parameters to be determined and a least-square method in combination with the Trust-region-reflective algorithm available in MATLAB (2011b) is employed to determine the appropriate values for them. The Trust-region-reflective algorithm refers to minimizing the value of a function, denoted as $g(x)$, by approximating $g(x)$ with a simpler function $p(x)$, which reasonably reflects the behavior of function $g(x)$ in a neighborhood N which is defined as the trust region. The key questions in defining a specific trust-region approach to minimizing $g(x)$ are how to choose and compute the approximation $p(x)$, how to choose and modify the trust region N, and how accurately to solve the trust-region problem. The objective herein is to minimize the root mean square, as indicated by Eq. (3).

$$J = \sum_{i=1}^{N} \sqrt{\frac{(F_{pi}-F_{ei})^2}{N}} \tag{3}$$

where N is the number of input-output pairs in each loop. F_p indicates the model-predicted output and F_e, the experimentally obtained output.

Table 1. Parameter values of the proposed MRE isolator model.

Parameters	A	α	β	γ	c_0	k_0
Values	0.62288	0.40962	0.30397	-0.47708	0.32774 N/(mm/sec)	14.542N/mm

Figure 9 shows the tracking process and relative errors of the predicted and measured forces with increasing time. It is observed that the relative error percentage is limited below 8%, which is acceptable in this modeling study. Figure 10 plots the comparison between the simulated and experimentally obtained responses. Figure 10(a) illustrates the force-displacement loop and Figure 10(b) describes the nonlinear relationship of force and velocity. It is obviously observed that the predicted behaviors resemble the experimental data very well, especially in the regions where the strain stiffening is obvious.

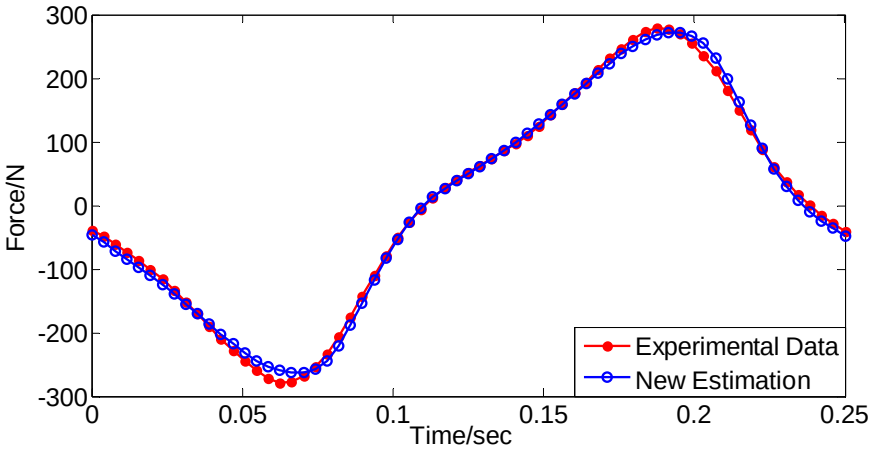

Figure 9. (a) Force vs. time.

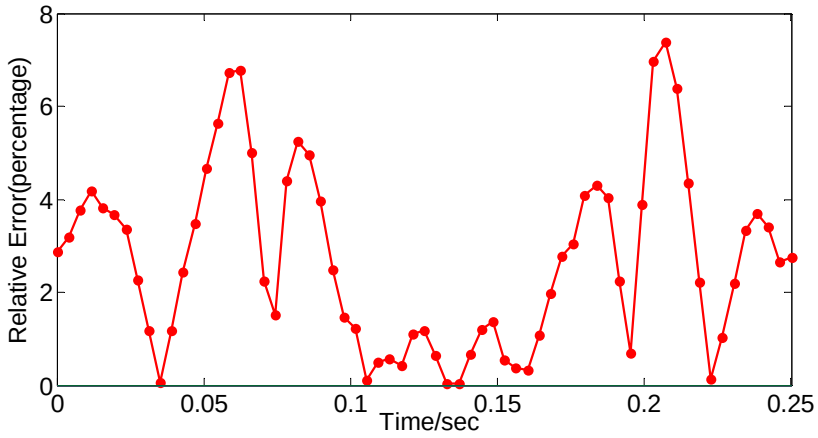

Figure 9. (b) Relative error vs. time.

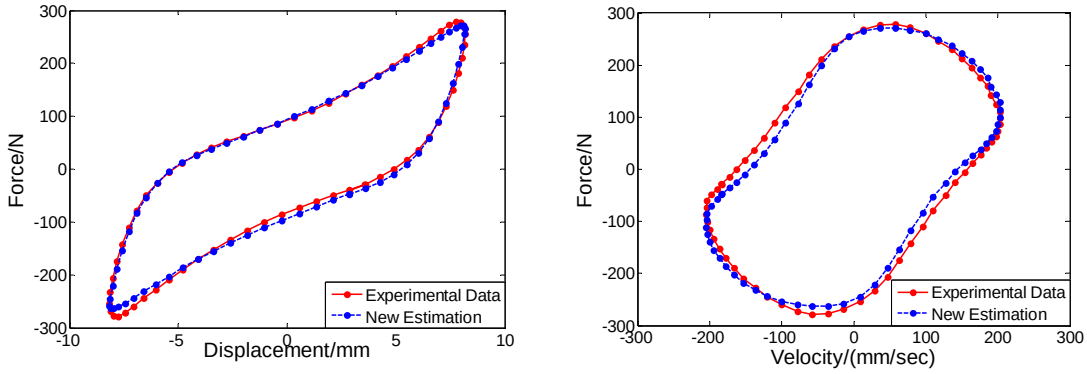

(a) Force vs. displacement (b) Force vs. velocity

Figure 10. Comparisons between the predicted and experimental responses.

To further validate the capability of the model for portraying the behaviors of the MRE isolator, more sets of comparisons between the predicted and measured data corresponding to different loading conditions are given in Figure 11. The new estimations presented in Figure

11(a) are optimized to fit the experimental data of 2 A - current, 4 Hz - frequency for 2mm, 4mm, and 8mm amplitudes respectively. It is seen that the experimentally measured responses are reasonably modeled. A closer look at the three predicted force-displacement loops illustrates that the effective stiffness reduces slightly as the amplitudes increases, demonstrating that the model is able to capture the Mullins Effect revealed in the experimental data. The measured force-displacement pairs shown in Figure 11(b) are obtained by loading the isolator with a 4 Hz sinusoid and an 8mm-amplitude at three current levels, 0 A, 1A, and 3 A, respectively. The three sets of comparisons verify the model's ability to describe the increasing nonlinearity of the hysteresis loops with the increasing currents. In particular, in each hysteresis loop, the predicted response resembles the unique behavior of straining hardening very well.

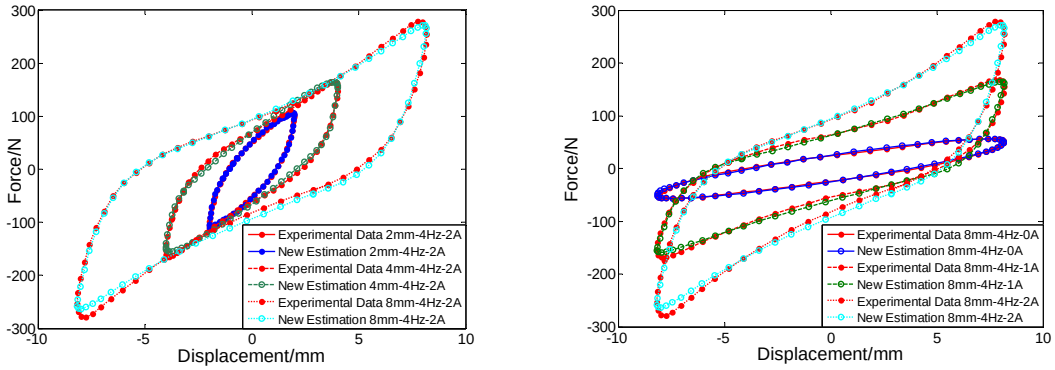

(a) Force vs. displacement (b) Force vs. velocity

Figure 11. Validation responses of the proposed MRE isolator model.

The predicted hysteresis loops change in the same regulation are summarised in Section 2.2. Besides some specific phenomena, for instance, strain stiffening, are captured, general rules are revealed in the figures as well. For example, the equivalent damping and maximum force change in an ascending way with the increasing amplitudes and currents, and also the increase in the current induces a large gain in the effective stiffness. All in all, Figure 11 further proves this proposed model is capable to accurately portray the MRE isolator's dynamics behaviors. Specifically, the predicted responses of the proposed model are matched the experimentally measured data of the MRE isolator when the current is in a constant level. Evidences provided verify the model's ability to accurately portray the behaviors of MRE isolator, especially in some specific regions. However, a versatile model is expected to achieve the unique performances of MRE isolator device when the fluctuating magnetic field is considered. To this end, a study on the field-dependent parameters is presented in the next section. Additionally, the effect of every single parameter on the sizes and shapes of hysteresis loops is discussed.

4. Field-Dependent Modeling and Discussion

In the proceeding section, the effect of fluctuating currents on the parameters in the proposed model is discussed and analyzed. Furthermore, the contribution of every parameter to the sizes and shapes of the predicted hysteresis loops is investigated.

Table 2 lists four groups of optimal values for the parameters of the proposed model described by (1) and (2). These values are identified using the experimental data obtained by loading the isolator with an 8 mm and 4 Hz sinusoidal signal at four current levels of 0 A, 1A, 2 A, and 3 A respectively. Among the four columns, the first one is chosen as the initial guess for the other three optimization processes. In each process, only one parameter is identified for three current levels. It is therefore that 18 cases in total have been conducted.

Table 2. Optimal values of parameters under different currents.

	0 A	1 A	2 A	3 A
A	0.0014419	0.095326	0.17508	0.24699
α	0.9916	0.63032	0.32596	0.12973
k_0 (N/mm)	5.6994	14.792	24.913	31.494
c_0 (N/(mm/sec))	0.1246	0.38192	0.59138	0.69734
γ	-3.3327	-3.6512	-3.7028	-3.7239
β	2.6644	2.3265	2.2756	2.2351

Figure 12 shows the relationships between the parameters and the current based on the listed values in Table 2. It is seen that these four parameters of A, α, k_0 and c_0 appear to vary linearly with the current. Therefore, the following relations are proposed:

$$A = A_a + A_b I, \alpha = \alpha_a + \alpha_b I, k_0 = k_{0a} + k_{0b} I \text{ and } c_0 = c_{0a} + c_{0b} I \qquad (4)$$

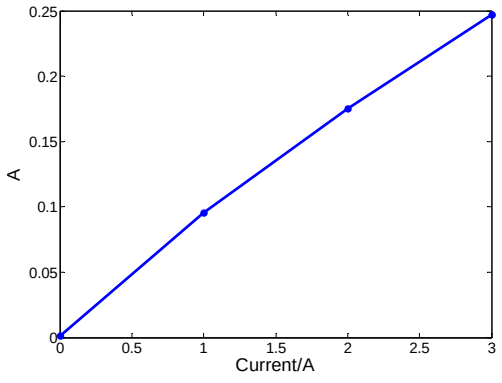

(a)A vs. current

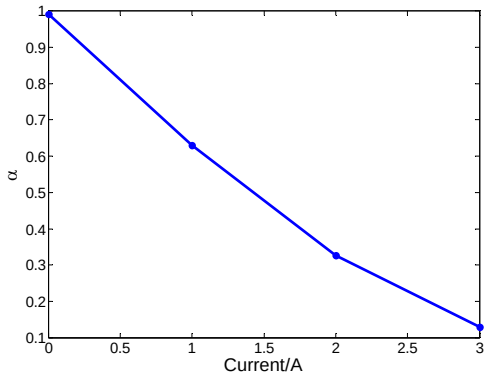

(b) α vs. current

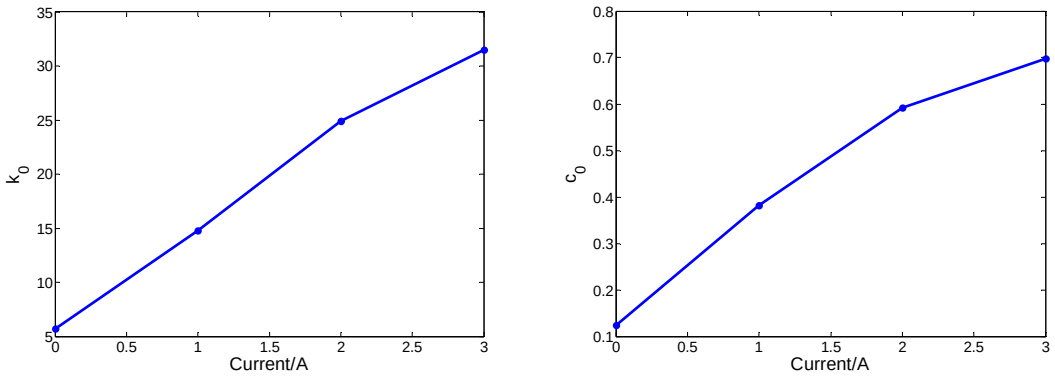

(a) $k_0$vs. current (b) c_0 vs. current

Figure 12. Relationships between parameters and current.

The optimal parameters for relationships in (4) are provided in Table 3. To validate the effectiveness of the field dependent parameters, comparison plots are presented in Figure 13, where the experimental data is from a loading of 4 mm and 4 Hz sinusoidal signal with the current of 1A. It can be seen from Figure 13 that the MRE isolator's behaviors are well captured.

Table 3. Optimal values for field dependent parameters.

Parameter	Value	Parameter	Value
A_a	0.80225	A_b	$1.5043I^{-1}$
α_a	0.15371	α_b	$0.28939I^{-1}$
k_{0a}	1.3103/(N/mm)	k_{0b}	3.322/(N*I/mm)
c_{0a}	0.044604/(N*sec/mm)	c_{0b}	0.087104/(N*sec*I/mm)
β	0.8549	γ	-0.91404

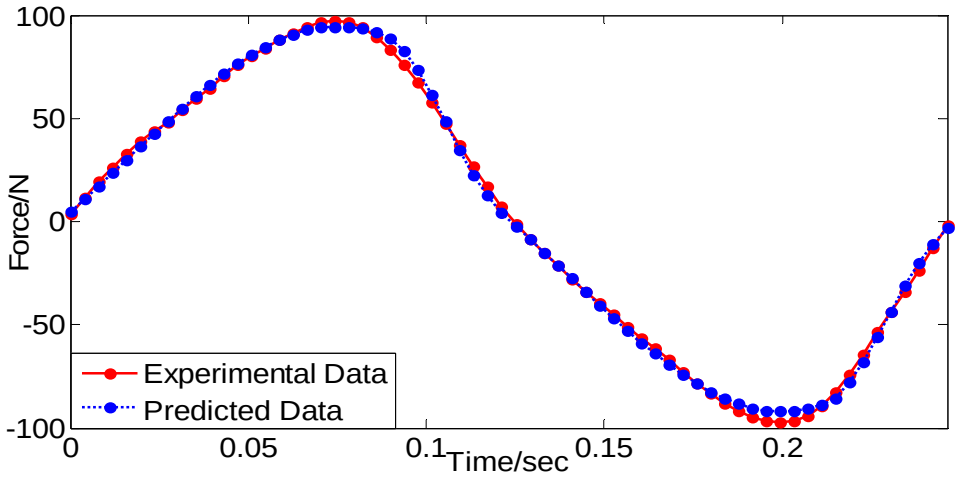

(a) Force vs. time

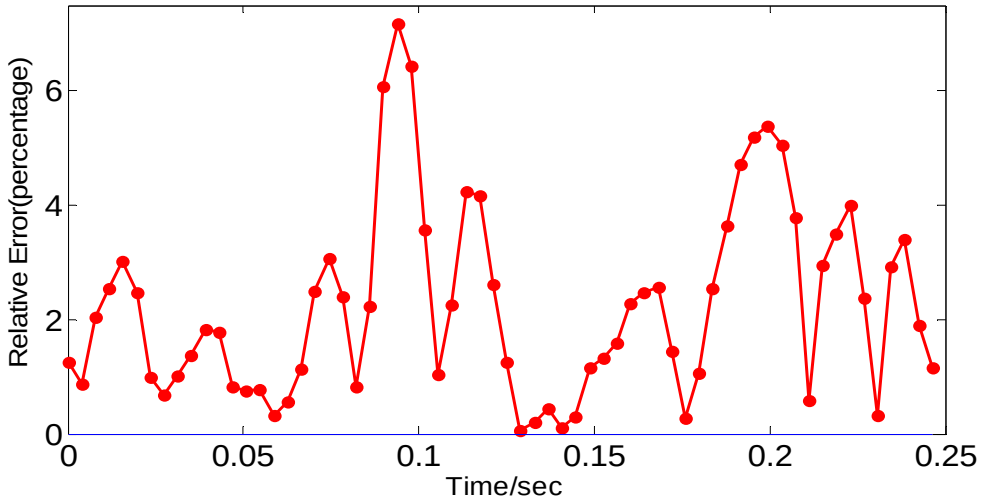

(b) Relative error vs. time.

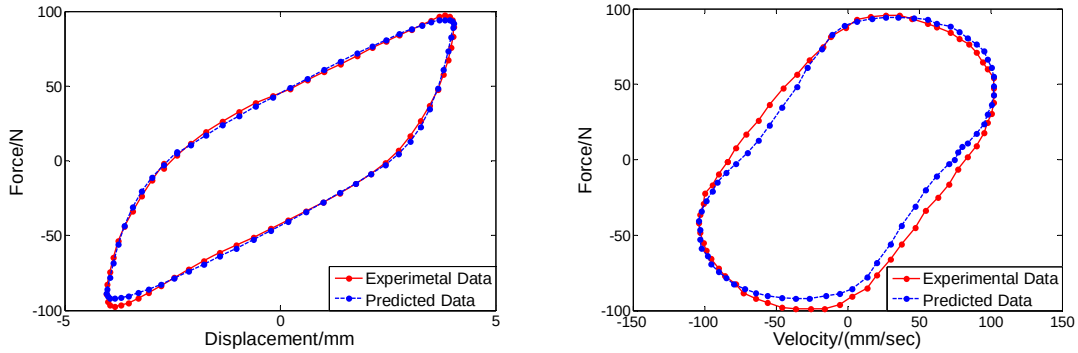

(c) Force vs. displacement

(d) Force vs. velocity

Figure 13. Comparisons between the predicted and experimentally measured response.

Taking the continuously varied currents into account makes this model more comprehensive for use, and meanwhile makes it easier to adjust parameters. Parameter adjustment after identification process helps improve the resemblance between the predicted and measured response, however, the influence of every parameter on the performances of the proposed model must be first investigated. In the following part, an effort to study the parameters' effects on the model output for the purpose of making it possible for the model to be easily controlled and adjusted is made. The optimized values listed in Table 1 are used as reference values. In each case among five cases, only one parameter is adjusted and the corresponding input-output pairs are collected and plotted to see variations of hysteresis loops.

As mentioned above, α indicates the linear degree of every hysteresis loop. For this reason, every value of α represents a hysteresis loop of different shape. Three sets of hysteresis loops corresponding to three α values, 0, 0.40962, and 1, respectively, are given, as shown in Figure 14.

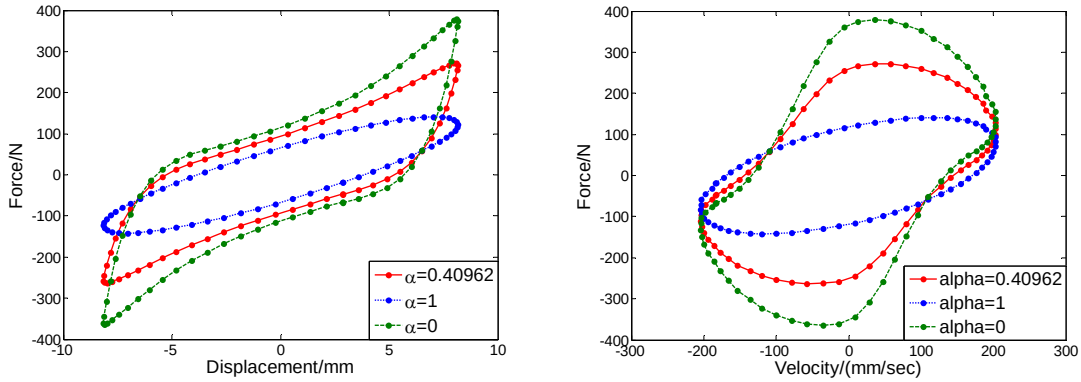

(a) Force vs. displacement (b) Force vs. velocity

Figure 14. α dependent responses of the proposed MRE isolator model.

When α equals to 1, the force function is simply represented in Eq. (5), it is observed from Figure 14 that the hysteresis loop is exactly an ellipse which presents a linear relationship. Instead, when α equals to zero corresponding to force function of Eq. (6), the nonlinearity of the hysteresis loop reaches the maximum degree. When α fluctuates in the range of $(0,1)$, the nonlinearity degree varies between the two extreme situations, namely linearity and maximum nonlinearity.

$$F = k_0 x + c_0 \dot{x} \tag{5}$$

$$F = k_0 z + c_0 \dot{x} \tag{6}$$

Similar to the force-displacement responses, the force-velocity response shows the same rule, i.e. the hysteresis loops tend to be more nonlinear with the descending values of α.

As can be seen from the force-velocity relationships shown in Figures 5-7, the output forces almost reach its maximum when the velocity is zero and decrease to its minimum when the velocity equals to its maximum. It is concluded that the damping force, indicated by $c_0\dot{x}$ in the force function, contributes a small part to the total force. The identified values of c_0 being very small support this conclusion. It is therefore reasonable that c_0 varies in a small range. Figure 15 presents four sets of hysteresis loops of different sizes and shapes corresponding to four different values of c_0. As might be expected, the effect of changing c_0 on the maximum force is slight. The other effect to be noted is that the sizes of the force-displacement loops tend to be thinner when c_0 is fixed at a small value than when c_0 is assigned a bigger one. Since the areas enclosed by the force-displacement loops indicate the equivalent damping, the change in the graphical curves matches the numerical variations.

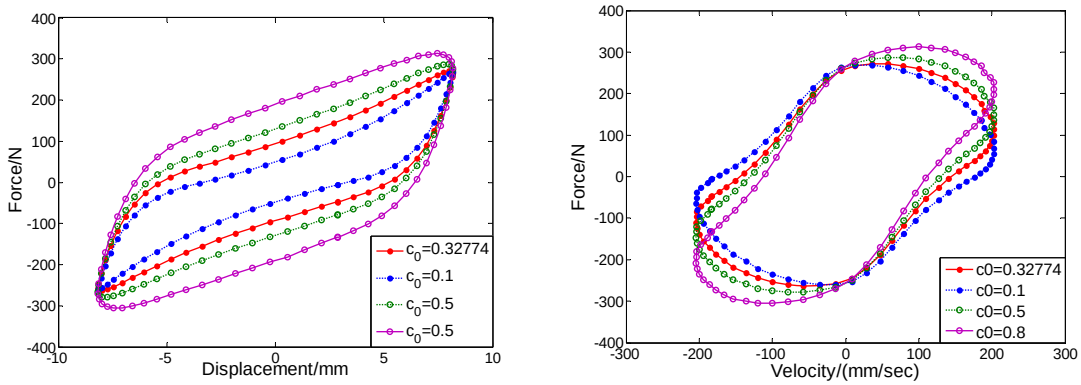

(a) Force vs. displacement (b) Force vs. velocity

Figure 15. c_0 dependent responses of the proposed MRE isolator model.

Figure 16 presents the resultant hysteresis loops by changing the values of k_0. It is seen that the maximum force and effective stiffness change almost linearly with k_0. Another phenomenon worth noting is that all the loops intersect at two points, as highlighted by M and N in Figure 16(a), from which the system stiffness under different k_0 becomes different. Furthermore, the two points indicate the critical points of strain stiffening, as observed in each loop strain stiffening tends to be obvious from these two points. In order to provide a more detailed explanation, the hysteresis loop can be divided into two parts, separated by the solid line. Take only the upper section for an example, as the force-displacement loops follow clockwise paths, it is noticed that the system stiffness of the left part of point M decreases as the hysteresis loop progresses, while the system stiffness of the right part tends to increase. It is therefore reasonably inferred that strain stiffening starts from point M. Additionally, the horizontal axis range for strain stiffening is from -2 mm to 8 mm. The same rule applies to point N and the strain stiffening range of the lower section is from 2 mm to -8 mm.

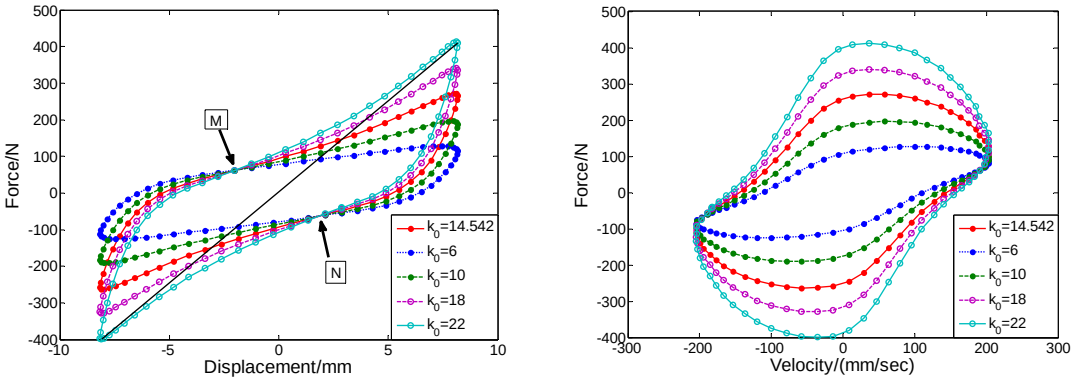

(a) Force vs. displacement (b) Force vs. velocity

Figure 16. k_0 dependent responses of the proposed MRE isolator model.

The effect of parameter A on the response shape is shown in Figure 17. It is noticed that the effect of adjusting A on hysteresis loops is very similar to that of changing k_0. Conclusions

includes that the maximum force and effective stiffness vary linearly with A, and two critical points for strain stiffening exist as well, donated by P and Q. However, the strain stiffening range is [-4, 8] mm and [-8, 4] mm respectively which is larger than that of k_0, indicating that A is more sensitive than k_0 to this model.

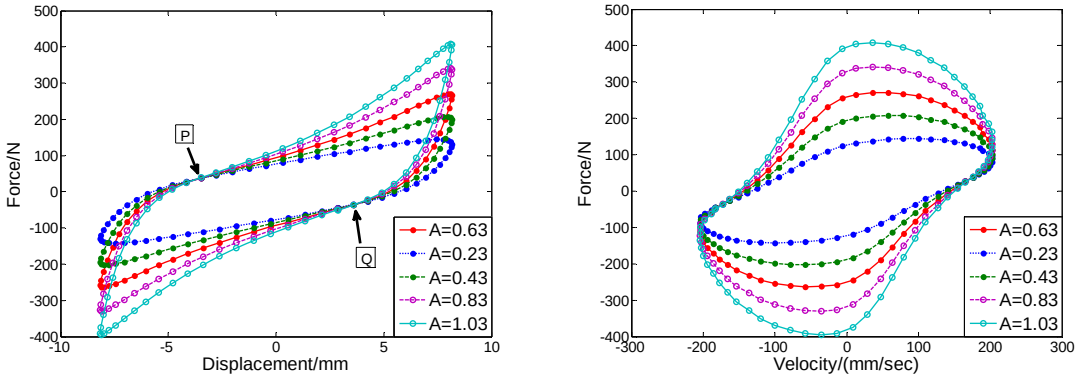

(a) Force vs. displacement (b) Force vs. velocity

Figure 17. *A* dependent responses of the proposed MRE isolator model.

β and γ have been recognized to shape the hysteresis loops. Figure 18 presents a series of hysteretic responses with respect to different β and γ. Figure 18(a) shows the effects of β on shaping hysteresis loops and Figure 18(b) shows that of γ. It is seen from Figure 18(a) that the nonlinearity tends to be more obvious as the value of β gets smaller. On the contrary, when β grows, the hysteretic shapes are inclined to be linear ellipses. One point needs to be emphasized is that when β is increased to a certain value, its influence on the shape is limited. As donated by an arrow in Figure 18(a), the hysteretic shapes remain an ellipse as the β increases from 1 to 2 with an increment of 0.2. Another important finding to add is that an effective β should be kept positive. In other words, β should fluctuate in an effective range for reproducing reasonable hysteretic shapes on condition that all the other referenced parameters are fixed. Speaking of the effect of γ, as noticed in Figure 18(b), it is very similar except minor differences to that of β. In the case when γ is negative, the nonlinearity level increases with the increasing absolute value of γ, otherwise, the hysteresis loops progress linearly. Also note that the responses remain linear when the value of γ is above zero.

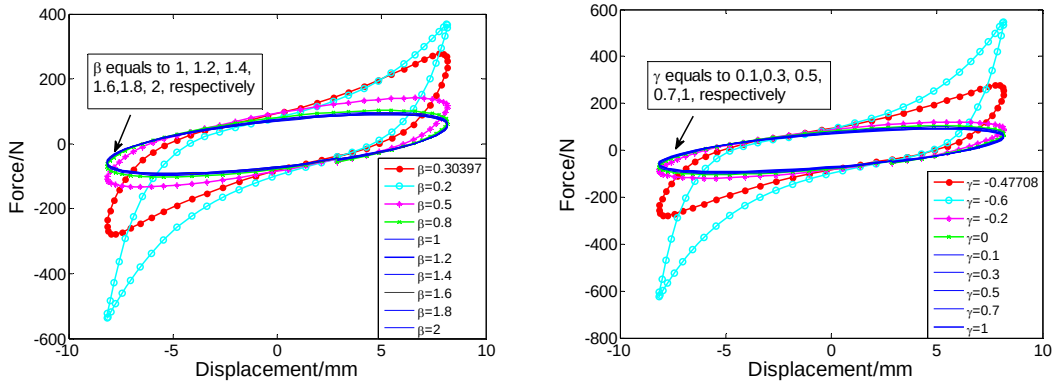

(a) Force vs. displacement (b) Force vs. displacement

Figure 18. β *and* γ dependent responses of the proposed MRE model.

Referring to the combinations of signs of $\beta+\gamma$ and $\gamma-\beta$, a leading study has been done in presenting five kinds of hysteretic shapes relating to five combinations of signs of $\beta+\gamma$ and $\gamma-\beta$. In this work, five cases will reappear for the purpose of validating the influence of β and γ on controlling the hysteresis loop shapes. For the reason that the hysteresis curves are produced by Eq. (2), it is natural the five cases will describe the relationship between the input displacement and the evolutionary variable z. Table 4 lists different values for β and γ to satisfy five combinations of $\beta+\gamma$ and $\gamma-\beta$ and the associated hysteretic shapes are plotted in Figure 19. As discussed above, β should be positive to be effective and γ has a wide variation range. Hence, the five cases are obtained by adjusting γ. It is clear that five different situations are presented as observed in reference [28]. And clearly the optimal values of $\beta+\gamma$ and $\gamma-\beta$ listed in Table 1 satisfies the combination of case one.

Table 4. Five combinations of $\beta+\gamma$ and $\gamma-\beta$.

Combinations			β	γ
Case 1	$\beta+\gamma>0$	$0<\gamma-\beta<\beta+\gamma$	0.1	0.3
Case2		$\gamma-\beta<0$	0.4	-0.3
Case3		$\gamma-\beta=0$	0.2	0.2
Case4	$\beta+\gamma=0$	$\gamma-\beta<0$	0.4	-0.4
Case5	$\beta+\gamma<0$	$\gamma-\beta<\beta+\gamma<0$	0.3	-0.6

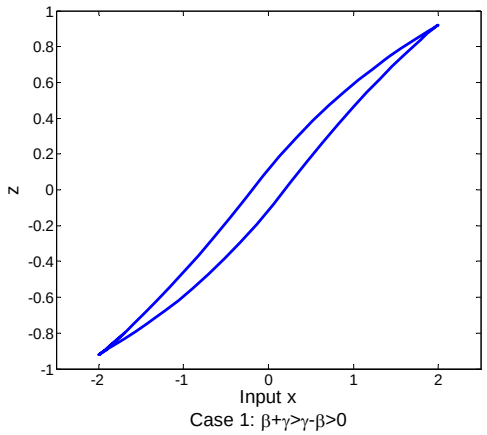

Case 1: β+γ>γ-β>0

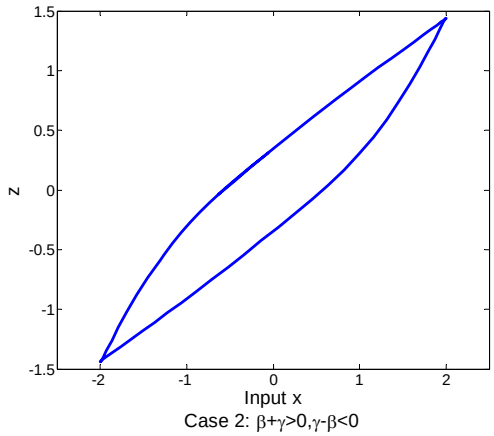

Case 2: β+γ>0,γ-β<0

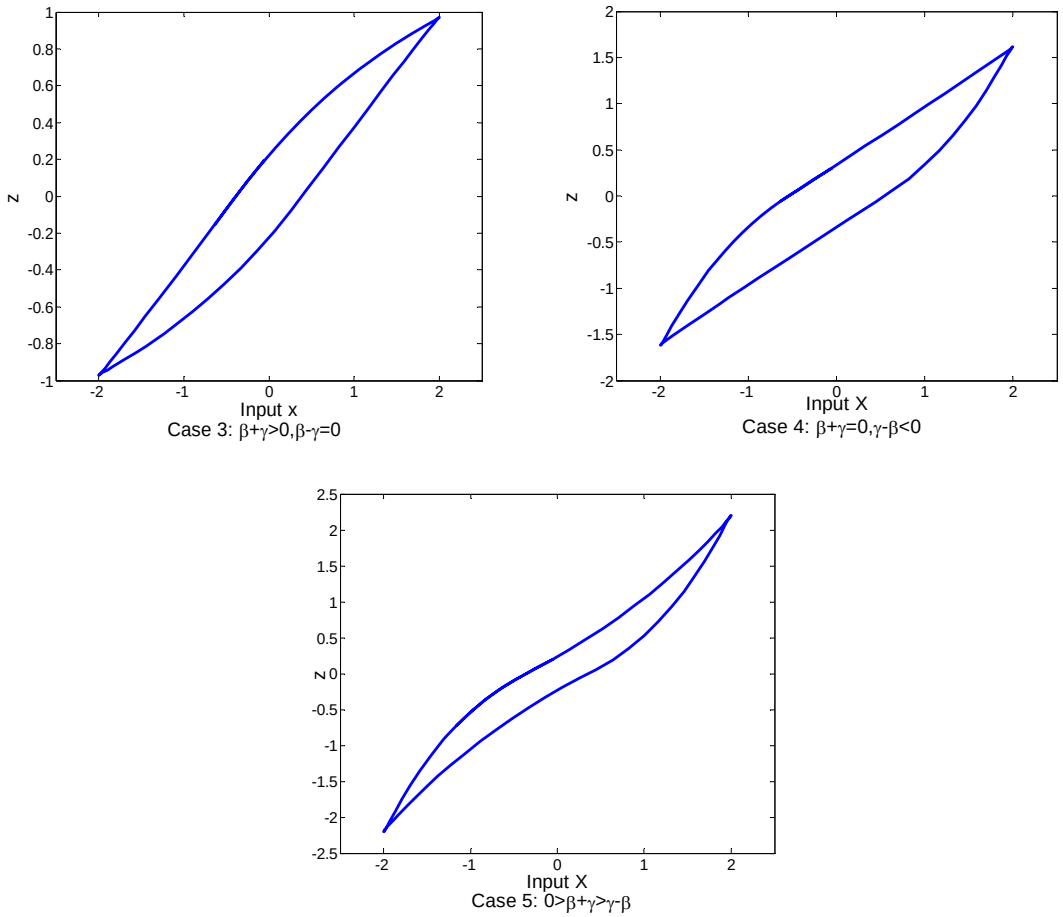

Figure 19. Different shapes for five kinds of combinations of β and γ.

5. Conclusion

A newly high-adjustable MRE seismic isolator was designed, fabricated and tested. The observed performances in experimental data reveal that the increase in loading amplitude leads to an increase in the damping capacity and maximum force but a light decrease in effective stiffness, that frequency poses minor influence on these three performance indicators, especially when it is above 0.1Hz, and that MRE exhibits field-dependent property that the effective stiffness and equivalent damping tend to increase with the progressively larger currents.

To take the maximum advantage of potential MRE material into control applications, a model for MRE isolator is developed. The resemblance between the predicted and measured response verify that the newly proposed model is competent to model the MRE isolator device. To make the proposed model more adaptive, the fluctuating magnetic field is taken into account. And the study on the dependence of the model to every parameter further improves the model to be more easily controlled and adjusted. Future work may focus on the advanced control algorithms and applications in suppressing vibrations of the model.

Acknowledgments

This research is supported by the University of Wollongong and China Scholarship Council joint scholarships, and National Natural Science Foundation of China (Grant No: 51328502, and 51205100).

References

1. Goodall, R.M., *Control engineering challenges for railway trains of the future.* Measurement and Control, 2011. **44**(1): p. 16-24.
2. Elbeheiry, E. and D. Karnopp, *Optimal control of vehicle random vibration with constrained suspension deflection.* Journal of Sound and Vibration, 1996. **189**(5): p. 547-564.
3. Symans, M., et al. *Semi-active fluid viscous dampers for seismic response control*. in *First World Conference on Structural Control*. 1994.
4. Patten, W., et al. *Suppression of vehicle induced bridge vibration via hydraulic semi-active vibration dampers*. in *Proc, First World Conf. on Struct. Control, FAI*. 1994.
5. Akbay, Z. and H. Aktan. *Actively regulated friction slip devices*. in *Proc., 6th Can. Conf. On Earthquake Engrg*. 1991.
6. Dowdell, D. and S. Cherry. *Semi-active friction dampers for seismic response control of structures*. in *Proc., Fifth US. Nat. Conf. on Earthquake Engrg*. 1994.
7. Kobori, T., et al., *Seismic response controlled structure with active variable stiffness system.* Earthquake engineering & structural dynamics, 1993. **22**(11): p. 925-941.
8. Jung, H., et al., *State-of-the-art of semiactive control systems using MR fluid dampers in civil engineering applications.* Structural Engineering and Mechanics, 2004. **17**(3-4): p. 493-526.
9. Lam, A.H.-F. and W.-H. Liao, *Semi-active control of automotive suspension systems with magneto-rheological dampers.* International Journal of Vehicle Design, 2003. **33**(1): p. 50-75.
10. Wang, D. and W. Liao, *Semi-active suspension systems for railway vehicles using magnetorheological dampers. Part I: system integration and modelling.* Vehicle System Dynamics, 2009. **47**(11): p. 1305-1325.
11. Stanway, R., J. Sproston, and N. Stevens, *Non-linear modelling of an electro-rheological vibration damper.* Journal of Electrostatics, 1987. **20**(2): p. 167-184.
12. Spencer, B., et al., *Phenomenological model for magnetorheological dampers.* Journal of engineering mechanics, 1997. **123**(3): p. 230-238.
13. Li, W., Y. Zhou, and T. Tian, *Viscoelastic properties of MR elastomers under harmonic loading.* Rheologica acta, 2010. **49**(7): p. 733-740.
14. Hoang, N., N. Zhang, and H. Du, *A dynamic absorber with a soft magnetorheological elastomer for powertrain vibration suppression.* Smart materials and structures, 2009. **18**(7): 074009.
15. Du, H., W. Li, and N. Zhang, *Semi-active variable stiffness vibration control of vehicle seat suspension using an MR elastomer isolator.* Smart materials and structures, 2011. **20**(10): 105003.
16. Liao, G., et al., *The design of an active–adaptive tuned vibration absorber based on magnetorheological elastomer and its vibration attenuation performance.* Smart materials and structures, 2011. **20**(7): 075015.
17. Deng, H.-x., X.-l. Gong, and L.-h. Wang, *Development of an adaptive tuned vibration absorber with magnetorheological elastomer.* Smart materials and structures, 2006. **15**(5): p. N111.
18. Ni, Z., et al., *Study on a dynamic stiffness-tuning absorber with squeeze-strain enhanced magnetorheological elastomer.* Journal of Intelligent Material Systems and Structures, 2009. **20**(10): p. 1195-1202.
19. Zhang, X. and W. Li, *Adaptive tuned dynamic vibration absorbers working with MR elastomers.* Faculty of Engineering-Papers, 2009: p. 517-529.
20. Li, Y., et al., *Development and characterization of a magnetorheological elastomer based adaptive seismic isolator.* Smart Materials and Structures, 2013. **22**(3): 035005.

21. Zhou, Y., W.H. Li, and M.N. Hadi, *Performance comparison between an MRF damper and an MRE isolator incorporated with a building structure.* Applied Mechanics and Materials, 2010. **37**: p. 862-865.
22. Li, Y., et al. *A highly adjustable magnetorheological elastomer base isolator for real-time adaptive control.* Smart Materials and Structures, 2013. **in press**.
23. Holt, W., *Behavior of rubber under repeated stresses.* Rubber Chemistry and Technology, 1932. **5**(1): p. 79-89.
24. Mullins, L., *Effect of stretching on the properties of rubber.* Rubber Chemistry and Technology, 1948. **21**(2): p. 281-300.
25. Mullins, L. and N. Tobin, *Theoretical model for the elastic behavior of filler-reinforced vulcanized rubbers.* Rubber Chemistry and Technology, 1957. **30**(2): p. 555-571.
26. Bueche, F., *Molecular basis for the Mullins effect.* Journal of Applied Polymer Science, 1960. **4**(10): p. 107-114.
27. Besdo, D. and J. Ihlemann, *Properties of rubberlike materials under large deformations explained by self-organizing linkage patterns.* International Journal of Plasticity, 2003. **19**(7): p. 1001-1018.
28. Sues, R., S. Mau, and Y.-K. Wen, *Systems identification of degrading hysteretic restoring forces.* Journal of engineering mechanics, 1988. **114**(5): p. 833-846.